Available online at www.sciencedirect.com
ScienceDirect
Journal of Computational Physics 227 (2008) 7643–7663
JOURNAL OF COMPUTATIONAL PHYSICS
www.elsevier.com/locate/jcp

On a numerical implementation of a formulation of anisotropic continuum elastoplasticity at finite strains

Carlo Sansour [a,*], Igor Karšaj [b], Jurica Sorić [b]

[a] The University of Nottingham, School of Civil Engineering, University Park, Nottingham NG7 2RD, UK
[b] Faculty of Mechanical Engineering and Naval Architecture, University of Zagreb, I. Lučića 5, HR-1000 Zagreb, Croatia

Received 9 September 2006; received in revised form 21 February 2008; accepted 25 April 2008
Available online 7 May 2008

Abstract

In a recent theoretical study [see C. Sansour, I. Karšaj, J. Sorić, A formulation of anisotropic continuum elastoplasticity at finite strains. Part I: Modelling, International Journal of Plasticity 22 (2006) 2346–2365], a constitutive model for anisotropic elastoplasticity at finite strains has been developed. The model is based on the multiplicative decomposition of the deformation gradient. The stored energy function as well as the flow rule has been considered as quadratic functions of their arguments. In both cases, the list of arguments is extended to include structural tensors which describe the anisotropy of the material response at hand. Non-linear isotropic hardening is considered as well. In this paper, the integration of the constitutive law is presented. The associative flow rule is integrated using the exponential map which preserves the plastic incompressibility condition. The numerical treatment of the problem is fully developed and expressions related to the local iteration and the consistent tangent operator are considered in detail. It is shown that while the consistent linearisation of the model is quite complicated, it still can be achieved if various intriguing implicit dependencies are identified and correctly dealt with. Various numerical examples of three-dimensional deformations of whole structural components are presented. The examples clearly illustrate the influence of anisotropy on finite elastoplastic deformations.

Keywords: Computational plasticity; Multiplicative inelasticity; Anisotropy; Finite strains; Exponential map

1. Introduction

In a recent study by Sansour et al. [13], a general thermodynamically consistent theory for anisotropic elastoplasticity at finite strains has been proposed. In this paper, we develop the numerical integration schemes and present numerical examples. Given the multiplicative structure of the theory, the development of appropriate numerical schemes is in fact an involved task. Some inelastic computations at finite strains involving anisotropy has been reported in the literature. In [11,17], the computations were based on additive decompositions of an appropriate strain measure without any reference to the multiplicative decomposition of the

* Corresponding author.
E-mail addresses: carlo.sansour@nottingham.ac.uk (C. Sansour), igor.karsaj@fsb.hr (I. Karšaj), jurica.soric@fsb.hr (J. Sorić).

0021-9991/$ - see front matter © 2008 Elsevier Inc. All rights reserved.
doi:10.1016/j.jcp.2008.04.025

deformation gradient. Additive decompositions preserve the simple structure of the linear theory. The theoretical framework can be straightforwardly developed, essentially by copying that of the linear theory. The same is true for the numerical schemes as well. However, the elegance and physical motivation assigned to the multiplicative decomposition remain lacking. The multiplicative decomposition itself has been employed in [10,3,6]. Beyond serious differences on the theoretical side between the treatments in the mentioned papers and ours, in the first two mentioned papers only numerically derived tangent operators where employed since consistent linearisation was considered too complicated or not available. The third paper was of rather theoretical nature. A consistent tangent operator was derived in [15,12], however, the anisotropy was only present in the elastic law while the flow rule was considered isotropic.

In this paper, we embark on a complete implementation of the theory. The integration of the flow rule is carried out using exponential map procedures as outlined in [16]. The use of the exponential map was first suggested in [4] for symmetric arguments and then extended to non-symmetric arguments in [14,16]. The task of model linearisation within numerical schemes is all but straightforward. Due to the multiplicative structure of the theory, various intriguing implicit dependencies must be first identified in order for the linearisation process to be correctly accomplished. This is true for the local iteration step as well as for the derivation of the consistent tangent operator. Both steps are presented in detail.

The theory and the computational algorithms have been implemented and applied to a shell finite element developed in [14,16]. The shell formulation allows for the use of complete three-dimensional constitutive laws. Accordingly, the deformations considered are always three-dimensional.

The paper is organized as follows. In Section 2, a summary of the theoretical framework is presented. Section 3 is devoted to the integration of the evolution equations; while Section 3.1 discusses the local iteration, Section 3.2 considers the derivation of the consistent elastoplastic tangent operator. In Section 4, various numerical examples are presented. The paper closes with some conclusions.

2. Summary of the theoretical framework

For details the reader is referred to [13]. Let $\mathbf{F}$ be the deformation gradient and

$$\mathbf{F} = \mathbf{F}_e \mathbf{F}_p \tag{1}$$

its corresponding decomposition into elastic and inelastic parts. Define the following strain-like tensors of right Cauchy–Green-type:

$$\mathbf{C} = \mathbf{F}^T \mathbf{F}, \tag{2}$$

$$\mathbf{C}_e = \mathbf{F}_e^T \mathbf{F}_e, \tag{3}$$

$$\mathbf{C}_p = \mathbf{F}_p^T \mathbf{F}_p, \tag{4}$$

where $\mathbf{C}_e$ defines the elastic strain tensor and $\mathbf{C}_p$ is its analogous plastic counterpart. Consider the rates of $\mathbf{F}$ and $\mathbf{F}_p$ defined by

$$\mathbf{L} = \mathbf{F}^{-1}\dot{\mathbf{F}}, \quad \mathbf{L}_p = \mathbf{F}_p^{-1}\dot{\mathbf{F}}_p, \tag{5}$$

and let $\boldsymbol{\tau}$ be the Kirchhoff stress tensor and $\boldsymbol{\Xi}$ its material counterpart (Eshelby-like) defined by

$$\boldsymbol{\Xi} = \mathbf{F}^T \boldsymbol{\tau} \mathbf{F}^{-T}. \tag{6}$$

The dissipation inequality

$$\mathcal{D} = \boldsymbol{\Xi} : \mathbf{L} - \rho_0 \dot{\psi}(\mathbf{C}_e, Z) \geqslant 0, \tag{7}$$

where ψ is the stored energy function, Z is an internal variable and ρ_0 the density at the reference configuration, can be reduced to the following statements. Two relationships for the thermodynamical forces:

$$\boldsymbol{\Xi} = 2\rho_0 \mathbf{C}\mathbf{F}_p^{-1} \frac{\partial \psi}{\partial \mathbf{C}_e} \mathbf{F}_p^{-T}, \tag{8}$$

$$Y = -\rho_0 \frac{\partial \psi}{\partial Z}, \tag{9}$$

and a reduced dissipation inequality

$$\mathcal{D}_r = \boldsymbol{\Xi} : \mathbf{L}_\mathrm{p} + Y \cdot \dot{Z} \geqslant 0. \tag{10}$$

We introduce the privileged directions of the material related to the elastic response as ${}_i\mathbf{v}_\mathrm{e},\ i = 1,2,3$, where the relations hold

$${}_i\mathbf{v}_\mathrm{e} \cdot {}_j\mathbf{v}_\mathrm{e} = \delta_{ij}, \tag{11}$$

with δ_{ij} as Kronecker's delta and a dot denoting scalar multiplication of vectors. Given the privileged directions, one defines the so-called structural tensors as the tensor products

$${}_i\mathbf{M}_\mathrm{e} = {}_i\mathbf{v}_\mathrm{e} \otimes {}_i\mathbf{v}_\mathrm{e}, \quad i = 1,2,3. \tag{12}$$

The free energy function is now assumed to be of the following quadratic form:

$$\rho_0 \psi_\mathrm{e} = \sum_{i=1}^{3} \left[\alpha_i J_i + \frac{1}{2} \sum_{j=1}^{3} \alpha_{(ij)} J_i J_j + \alpha_{(i+9)} J_{(i+3)} \right]. \tag{13}$$

Here the invariants J_i and $J_{(i+3)}$ are defined according to

$$J_i = \mathrm{tr}[({}_i\mathbf{M}_\mathrm{e})\mathbf{C}_\mathrm{e}], \quad J_{(i+3)} = \mathrm{tr}[({}_i\mathbf{M}_\mathrm{e})\mathbf{C}_\mathrm{e}^2], \quad i = 1,2,3 \tag{14}$$

Herein $\alpha_i, \alpha_{(ij)}, \alpha_{i+9}$ are material constants, where $\alpha_{ij} = \alpha_{ji}$. We use also the alternative numbering: $\alpha_{(11)} = \alpha_4,\ \alpha_{(22)} = \alpha_5,\ \alpha_{(33)} = \alpha_6,\ \alpha_{(12)} = \alpha_{(21)} = \alpha_7,\ \alpha_{(13)} = \alpha_{(31)} = \alpha_8,\ \alpha_{(23)} = \alpha_{(32)} = \alpha_9$. Note that a general non-linear formulation of the free energy function in terms of the invariants $J_{(i+3)}$ does not insure polyconvexity, of relevance for the existence of solutions. However, the present formulation restricts the same invariant to a linear term, which is completely sufficient to describe the behaviour of metals of interest in the present study. Accordingly, the issue of polyconvexity of the free energy function is not relevant in the present restricted context.

With the explicit form of the free energy function, the evaluation of (8) results in the expression

$$\boldsymbol{\Xi} = 2\rho_0 \left\{ \sum_{i=1}^{3} \left[\frac{\partial \psi}{\partial J_i} \mathbf{C}\mathbf{C}_\mathrm{p}^{-1}({}_i\overline{\mathbf{M}}_\mathrm{e}) + \frac{\partial \psi}{\partial J_{(i+3)}} (\mathbf{C}\mathbf{C}_\mathrm{p}^{-1}({}_i\overline{\mathbf{M}}_\mathrm{e})\mathbf{C}\mathbf{C}_\mathrm{p}^{-1} + \mathbf{C}\mathbf{C}_\mathrm{p}^{-1}\mathbf{C}\mathbf{C}_\mathbf{p}^{-1}({}_i\overline{\mathbf{M}}_\mathrm{e})) \right] \right\} \tag{15}$$

Here, $({}_i\overline{\mathbf{M}}_\mathrm{e})$ are modified structural tensors defined by

$$({}_i\overline{\mathbf{M}}_\mathrm{e}) = \mathbf{F}_\mathrm{p}^\mathrm{T}({}_i\mathbf{M}_\mathrm{e})\mathbf{F}_\mathrm{p}^{-\mathrm{T}}, \quad i = 1,2,3. \tag{16}$$

For a better physical interpretation and experimental validation, it is useful to redefine the material constants. In comparison with more classical elasticity constants, which can be found in any text book, e.g. [9], the material parameters take

$$\alpha_4 = \frac{1}{4}\left(\frac{1 - \nu_{23}\nu_{32}}{2E_2E_3\Delta} - G_{12} - G_{13} + G_{23} \right), \tag{17}$$

$$\alpha_5 = \frac{1}{4}\left(\frac{1 - \nu_{31}\nu_{13}}{2E_3E_1\Delta} - G_{12} + G_{13} - G_{23} \right), \tag{18}$$

$$\alpha_6 = \frac{1}{4}\left(\frac{1 - \nu_{12}\nu_{21}}{2E_1E_2\Delta} + G_{12} - G_{13} - G_{23} \right), \tag{19}$$

$$\alpha_7 = \frac{\nu_{12} + \nu_{13}\nu_{32}}{4E_3E_1\Delta}, \tag{20}$$

$$\alpha_8 = \frac{\nu_{13} + \nu_{12}\nu_{23}}{4E_2E_3\Delta}, \tag{21}$$

$$\alpha_9 = \frac{\nu_{23} + \nu_{13}\nu_{21}}{4E_1E_2\Delta}, \tag{22}$$

$$\alpha_{10} = \frac{1}{8}(G_{12} + G_{13} - G_{23}), \tag{23}$$

$$\alpha_{11} = \frac{1}{8}(G_{12} - G_{13} + G_{23}), \tag{24}$$

$$\alpha_{12} = \frac{1}{8}(-G_{12} + G_{13} + G_{23}), \tag{25}$$

$$\alpha_1 = -(\alpha_4 + \alpha_7 + \alpha_8 + 2\alpha_{10}), \tag{26}$$

$$\alpha_2 = -(\alpha_5 + \alpha_7 + \alpha_9 + 2\alpha_{11}), \tag{27}$$

$$\alpha_3 = -(\alpha_6 + \alpha_8 + \alpha_9 + 2\alpha_{12}). \tag{28}$$

In the above relations, E_i, v_{ij} and G_{ij} denote the elastic constants related to the three different directions of orthotropy. Furthermore, Δ is abbreviation for the following expression

$$\Delta = \frac{1 - v_{12}v_{21} - v_{23}v_{32} - v_{31}v_{13} - 2v_{12}v_{23}v_{31}}{E_1E_2E_3}. \tag{29}$$

Having established the expression for the stress tensor, the flow rule follows. First the yield function is defined by

$$\phi = \sqrt{\frac{2}{3}}[\sigma_{11}^0\sqrt{\chi} - (\sigma_{11}^0 - Y)], \tag{30}$$

$$\chi = \sum_{i=1}^{3}\left[\beta_i I_i^2 + \beta_{(i+6)}I_{(i+3)} + \frac{1}{2}\sum_{j=1}^{3}\beta_{(i+j+1)}I_iI_j\right] \quad \text{for } i \neq j, \tag{31}$$

and the non-linear isotropic hardening by

$$Y = -HZ - (\sigma_\infty - \sigma_{11}^0)[1 - \exp(-\eta Z)]. \tag{32}$$

The scalar σ_{11}^0 as well as $\beta_1 - \beta_{12}$ are material constants. Furthermore, H is the linear isotropic hardening parameter, σ_∞ is the saturation yield stress, η is a constitutive parameter quantifying the rate at which the saturation yield stress is attained during loading The yield function itself is assumed to depend on the invariants

$$I_i = \mathrm{tr}[({}_i\mathbf{M}_y)\mathrm{dev}\,\boldsymbol{\Xi}], \quad I_{(i+3)} = \mathrm{tr}[({}_i\mathbf{M}_y)(\mathrm{dev}\,\boldsymbol{\Xi})^2], \quad i = 1,2,3, \tag{33}$$

where the structural tensors related to the plastic flow are

$${}_i\mathbf{M}_y = {}_i\mathbf{v}_y \otimes {}_i\mathbf{v}_y, \quad i = 1,2,3, \tag{34}$$

and ${}_i\mathbf{v}_y$ as the privileged directions of the plastic flow where the relations hold

$${}_i\mathbf{v}_y \cdot {}_j\mathbf{v}_y = \delta_{ij}, \tag{35}$$

which may differ from those defined for the elastic response. Clearly, the privileged directions of the material $\mathbf{v}_e, \mathbf{v}_y$ must be given a priori when defining the problem at hand. As all material parameters of a specific specimen they must be determined by experiments. In the examples considered in Section 4, the directions are given by an angle and a plane (the directions are orthogonal and so one angle in a plane is sufficient to define the directions).

The evolution equations now read

$$\mathbf{L}_\mathrm{p} = \lambda\frac{\partial\phi}{\partial\boldsymbol{\Xi}} = \lambda\boldsymbol{v} \Rightarrow \boldsymbol{v} = \sqrt{\frac{2}{3}}\frac{\sigma_{11}^0}{2\sqrt{\chi}}\frac{\partial\chi}{\partial\mathrm{dev}\,\boldsymbol{\Xi}}\frac{\partial\mathrm{dev}\,\boldsymbol{\Xi}}{\partial\boldsymbol{\Xi}}, \tag{36}$$

$$\dot{Z} = \lambda\frac{\partial\phi}{\partial Y} \Rightarrow \dot{Z} = \sqrt{\frac{2}{3}}\lambda, \tag{37}$$

where

$$\frac{\partial \chi}{\partial \operatorname{dev}\boldsymbol{\Xi}} = \sum_{i=3}^{3}\left[2\beta_i I_i({}_i\mathbf{M}_y) + \beta_{(i+6)}(\operatorname{dev}\boldsymbol{\Xi}^{\mathrm{T}}({}_i\mathbf{M}_y) + ({}_i\mathbf{M}_y)\operatorname{dev}\boldsymbol{\Xi}^{\mathrm{T}}) + \frac{1}{2}\sum_{j=1}^{3}\beta_{(i+j+1)}(({}_i\mathbf{M}_y)I_j + I_i({}_j\mathbf{M}_y))\right], \quad \text{for } i \neq j. \tag{38}$$

Herein, λ is plastic multiplier.

In comparison with experimental values, the material parameters can be determined to

$$\beta_1 = \frac{1}{(\sigma_{11}^0)^2} - \frac{1}{2}\left(\frac{1}{(\sigma_{12}^0)^2} + \frac{1}{(\sigma_{13}^0)^2} - \frac{1}{(\sigma_{23}^0)^2}\right), \tag{39}$$

$$\beta_2 = \frac{1}{(\sigma_{22}^0)^2} - \frac{1}{2}\left(\frac{1}{(\sigma_{12}^0)^2} - \frac{1}{(\sigma_{13}^0)^2} + \frac{1}{(\sigma_{23}^0)^2}\right), \tag{40}$$

$$\beta_3 = \frac{1}{(\sigma_{33}^0)^2} - \frac{1}{2}\left(-\frac{1}{(\sigma_{12}^0)^2} + \frac{1}{(\sigma_{13}^0)^2} + \frac{1}{(\sigma_{23}^0)^2}\right), \tag{41}$$

$$\beta_4 = -\left(\frac{1}{(\sigma_{11}^0)^2} + \frac{1}{(\sigma_{22}^0)^2} - \frac{1}{(\sigma_{33}^0)^2}\right), \tag{42}$$

$$\beta_5 = -\left(\frac{1}{(\sigma_{11}^0)^2} - \frac{1}{(\sigma_{22}^0)^2} + \frac{1}{(\sigma_{33}^0)^2}\right), \tag{43}$$

$$\beta_6 = -\left(-\frac{1}{(\sigma_{11}^0)^2} + \frac{1}{(\sigma_{22}^0)^2} + \frac{1}{(\sigma_{33}^0)^2}\right), \tag{44}$$

$$\beta_7 = \frac{1}{2}\left(\frac{1}{(\sigma_{12}^0)^2} + \frac{1}{(\sigma_{13}^0)^2} - \frac{1}{(\sigma_{23}^0)^2}\right), \tag{45}$$

$$\beta_8 = \frac{1}{2}\left(\frac{1}{(\sigma_{12}^0)^2} - \frac{1}{(\sigma_{13}^0)^2} + \frac{1}{(\sigma_{23}^0)^2}\right), \tag{46}$$

$$\beta_9 = \frac{1}{2}\left(-\frac{1}{(\sigma_{12}^0)^2} + \frac{1}{(\sigma_{13}^0)^2} + \frac{1}{(\sigma_{23}^0)^2}\right). \tag{47}$$

The values σ_{ij}^0 are experimental values and indicate the flow stress in different direction. In the following box, we summarize the theoretical framework:

Kinematics:

$$\mathbf{F} = \mathbf{1} + \operatorname{Grad}\mathbf{u}, \quad \mathbf{C} = \mathbf{F}^{\mathrm{T}}\mathbf{F}, \quad \mathbf{C}_{\mathrm{p}} = \mathbf{F}_{\mathrm{p}}^{\mathrm{T}}\mathbf{F}_{\mathrm{p}}, \quad \mathbf{L}_{\mathrm{p}} = \mathbf{F}_{\mathrm{p}}^{-1}\dot{\mathbf{F}}_{\mathrm{p}}$$

Elastic law:

$$\rho_0\psi_{\mathrm{e}} = \sum_{i=1}^{3}\left[\alpha_i J_i + \frac{1}{2}\sum_{j=1}^{3}\alpha_{(ij)}J_i J_j + \alpha_{(i+9)}J_{(i+3)}\right]$$

$$J_i = \operatorname{tr}[({}_i\mathbf{M}_{\mathrm{e}})\mathbf{C}_{\mathrm{e}}], \quad J_{(i+3)} = \operatorname{tr}[({}_i\mathbf{M}_{\mathrm{e}})\mathbf{C}_{\mathrm{e}}^2], \quad i = 1,2,3$$

$$\boldsymbol{\Xi} = 2\rho_0\left\{\sum_{i=1}^{3}\left[\frac{\partial\psi_{\mathrm{e}}}{\partial J_i}\mathbf{C}\mathbf{C}_{\mathrm{p}}^{-1}({}_i\overline{\mathbf{M}}_{\mathrm{e}}) + \frac{\partial\psi_{\mathrm{e}}}{\partial J_{(i+3)}}(\mathbf{C}\mathbf{C}_{\mathrm{p}}^{-1}({}_i\overline{\mathbf{M}}_{\mathrm{e}})\mathbf{C}\mathbf{C}_{\mathrm{p}}^{-1} + \mathbf{C}\mathbf{C}_{\mathrm{p}}^{-1}\mathbf{C}\mathbf{C}_{\mathrm{p}}^{-1}({}_i\overline{\mathbf{M}}_{\mathrm{e}}))\right]\right\}$$

$$({}_i\overline{\mathbf{M}}_{\mathrm{e}}) = \mathbf{F}_{\mathrm{p}}^{\mathrm{T}}({}_i\mathbf{M}_{\mathrm{e}})\mathbf{F}_{\mathrm{p}}^{-\mathrm{T}}, \quad ({}_i\mathbf{M}_{\mathrm{e}}) = {}_i\mathbf{v}_{\mathrm{e}} \otimes {}_i\mathbf{v}_{\mathrm{e}}, \quad i = 1,2,3$$

Flow rule:

$$\phi = \sqrt{\frac{2}{3}}\left[\sigma_{11}^{0}\sqrt{\chi} - \left(\sigma_{11}^{0} - Y\right)\right]$$

$$\chi = \sum_{i=1}^{3}\left[\beta_i I_i^2 + \beta_{(i+6)} I_{(i+3)} + \frac{1}{2}\sum_{j=1}^{3}\beta_{(i+j+1)} I_i I_j\right], \quad i \neq j$$

$$I_i = \mathrm{tr}[({}_i\mathbf{M}_y)\mathrm{dev}\,\boldsymbol{\Xi}], \quad I_{i+3} = \mathrm{tr}[({}_i\mathbf{M}_y)(\mathrm{dev}\,\boldsymbol{\Xi})^2], \quad i = 1,2,3$$

$$({}_i\mathbf{M}_y) = {}_i\mathbf{v}_y \otimes {}_i\mathbf{v}_y, \quad i = 1,2,3,$$

$$\mathbf{L}_{\mathrm{p}} = \lambda \boldsymbol{v}, \quad \dot{Z} = \sqrt{\frac{2}{3}}\lambda$$

$$\boldsymbol{v} = \sqrt{\frac{2}{3}}\frac{\sigma_{11}^{0}}{2\sqrt{\chi}}\mathrm{dev}\left\{\sum_{i=3}^{3}\left[2\beta_i I_i ({}_i\mathbf{M}_y)^{\mathrm{T}} + \beta_{(i+6)}(({}_i\mathbf{M}_y)\mathrm{dev}\,\boldsymbol{\Xi} + ({}_i\mathbf{M}_y)^{\mathrm{T}}\mathrm{dev}\,\boldsymbol{\Xi}) + \frac{1}{2}\sum_{j=1}^{3}\beta_{(i+j+1)}(({}_i\mathbf{M}_y)^{\mathrm{T}} I_j + I_i({}_j\mathbf{M}_{\mathbf{y}})^{\mathrm{T}})\right]\right\}, \quad \text{for } i \neq j$$

Box 1: Summary of the theory

We recall a result discussed in the theoretical part of this work that the theory is not invariant with respect to superimposed rotations on $\mathbf{F}_{\mathrm{p}}$. In fact, an underlying assumption is that the inelastic deformation does not influence the elastic response. The validity of such an assumption could be questioned. In fact, the importance of the numerical implementation to follow is that it give us means to test such assumptions by comparing the numerical results against either experiments or further numerical results achieved by means of alternative theoretical frameworks.

3. Integration algorithm

The constitutive equations are integrated using the well known predictor–corrector method. For any two time steps $[t_n, t_{n+1}]$ with the time increment $\Delta T = t_{n+1} - t_n$, the displacements and internal variables are assumed to be known at time step t_n and they have to be determined for t_{n+1}. First the constitutive law is assumed to be elastic with frozen internal variables (trial step). In the plastic corrector step, the right Cauchy–Green tensor $\mathbf{C}$ is held fixed while the internal variables are updated so as to fulfill the inelastic constitutive laws. While this idea is classic and is used in most inelastic computations it has never been applied to anisotropic multiplicative computations. It is this multiplicative structure with the full anisotropy which renders its realisation especially complicated and cumbersome. In both steps, the trial and the corrector step, linearisation processes are to be performed which have never been employed so far. In order to achieve quadratic convergence the linearisation must be performed correctly. Extreme care is to be exercised in order to achieve the goal as many nested and complicated dependencies exist which have to be meticulously dealt with. The linearisation process is of great importance for general non-homogenous large deformations. Computations of this type are very sensitive to the quality of the tangent operators employed. Out of these reasons, we believe that it is worthwhile to develop the numerical procedures in full, which is to happen in the next subsections.

The understanding that the unimodular tensor $\mathbf{F}_{\mathrm{p}}$ is an element of the Lie group $SL^{+}(3,\mathbb{R}^3)$, while $\mathbf{L}_{\mathrm{p}}$ is an element of the corresponding Lie algebra, motivates the use of the exponential map for time integration

$$\mathbf{F}_{\mathrm{p}}^{-1}|_{n+1} = \exp(-\Delta T \mathbf{L}_{\mathrm{p}})\mathbf{F}_{\mathrm{p}}^{-1}|_{n}. \tag{48}$$

The reader may recall that Lie groups are transformation groups (matrices) with certain features. The unimodular group is the group of matrices with determinant equals one. The term algebra of the group designates its rates. The algebra of $SL^{+}(3,\mathbb{R}^3)$ constitutes of matrices with vanishing traces. By the fact that $\det\exp(-\Delta T\mathbf{L}_{\mathrm{p}}) = \exp(-\Delta T\mathrm{tr}\mathbf{L}_{\mathrm{p}}) = \exp(\mathbf{0}) = \mathbf{1}$, the condition of plastic incompressibility is preserved exactly. The exponential map has been introduced by Weber and Anand [19] and Eterovic and Bathe [4] to integrate

inelastic flow rules, where approximate evaluations of the exponential map with symmetric arguments were carried out. An evaluation of the exponential map with non-symmetric arguments, up to an arbitrary accuracy, was given in [14]. This scheme is adopted in this paper as well. The derivative of the exponential map with respect to its argument is computed following a suggestion in [16].

3.1. Local iteration

The trial step provides us with the value of $\mathbf{C}$. Within a finite element formulation, at every integration point we wish to calculate an updated value for the elastic strain measure $\mathbf{C}\mathbf{C}_{\mathrm{p}}^{-1}$, which reads

$$\mathbf{C}\mathbf{C}_{\mathrm{p}}^{-1}|_{n+1} = \mathbf{C}|_{n+1} \exp(-\Delta T \mathbf{L}_{\mathrm{p}}) \mathbf{C}_{\mathrm{p}}^{-1}|_{n} \exp(-\Delta T \mathbf{L}_{\mathrm{p}}^{\mathrm{T}}). \tag{49}$$

This quantity determines the stress tensor. On the other hand, the rate $\mathbf{L}_{\mathrm{p}}$ itself, as given in (36), depends on the stress. Accordingly, a full iteration process is necessary to determine the inelastic rate such that the flow rule is not violated. The guiding principle is to calculate the correct value of the plastic multiplier λ through a full Newton–Raphson iteration. As no co-axiality between the rate and the stress exists, the dependencies of the yield function ϕ on tensorial components must be taken into account. Note that during the iteration not only the value but the direction of the stress will change as well.

At any iteration step, say $i+1$, the new value of λ is given as

$$\lambda|_{i+1} = \lambda|_{i} + \Delta\lambda. \tag{50}$$

Following Eq. (37), the value of $\lambda|_{n+1}$ at the end of the iteration cycle (time step $n+1$) determines the new internal variable Z as well

$$Z|_{n+1} = Z|_{n} + \sqrt{\frac{2}{3}} \Delta T \lambda|_{n+1}. \tag{51}$$

The calculation of $\Delta\lambda$ is based on the linearisation of Eq. (30). Accordingly, one has

$$\left(\frac{\partial \phi}{\partial \boldsymbol{\Xi}} \frac{\partial \boldsymbol{\Xi}}{\partial \lambda} + \frac{\partial \phi}{\partial Y} \frac{\partial Y}{\partial \lambda} \right) \Big|_{i} \cdot \Delta\lambda = -\phi|_{i}, \tag{52}$$

$$\Delta\lambda = -\left(\frac{\partial \phi}{\partial \boldsymbol{\Xi}} \frac{\partial \boldsymbol{\Xi}}{\partial \lambda} + \frac{\partial \phi}{\partial Y} \frac{\partial Y}{\partial \lambda} \right)^{-1} \Big|_{i} \phi|_{i}. \tag{53}$$

Some of the terms involved in this equation can be calculated in a straightforward manner. Using Eqs. (30) and (32) one has

$$\frac{\partial \phi}{\partial \boldsymbol{\Xi}} = \sqrt{\frac{2}{3}} \sigma_{11}^{0} \frac{1}{2\sqrt{\chi}} \frac{\partial \chi}{\partial \operatorname{dev} \boldsymbol{\Xi}} \frac{\partial \operatorname{dev} \boldsymbol{\Xi}}{\partial \boldsymbol{\Xi}}, \tag{54}$$

$$\frac{\partial \phi}{\partial Y} = \sqrt{\frac{2}{3}}, \tag{55}$$

$$\frac{\partial Y}{\partial \lambda} = -\sqrt{\frac{2}{3}} \Delta T [H + \eta(\sigma_{\infty} - \sigma_{Y}) \exp(-\eta Z|_{n+1})]. \tag{56}$$

The term $\partial\chi/\partial \operatorname{dev}\boldsymbol{\Xi}$ is known from (38). More involved is the term $\partial\boldsymbol{\Xi}/\partial\lambda$ to which we now turn our attention.

In the following and in an effort to make the operations transparent, index notation will be used throughout. Now, $\boldsymbol{\Xi}$ depends on $\mathbf{C}$ and $\mathbf{C}_{\mathrm{p}}^{-1}$. During the local iteration, $\mathbf{C}$ is fixed and so is not a variable. On the other hand, $\mathbf{C}_{\mathrm{p}}^{-1}$ depends on $\mathbf{F}_{\mathrm{p}}^{-1}$, which, through (48), depends on $\mathbf{L}_{\mathrm{p}}$. The latter depends, via Eq. $(36)_1$, on λ in two different ways. First, explicitly and, second, implicitly through the dependency of $\boldsymbol{v}$ on $\boldsymbol{\Xi}$, the dependency of which on λ we are seeking. With theses explicit and implicit dependencies, $\partial\boldsymbol{\Xi}/\partial\lambda$ reads

$$\frac{\partial \Xi_{c}^{d}}{\partial \lambda} = \frac{\partial \Xi_{c}^{d}}{\partial (\mathbf{L}_{\mathrm{p}})_{f}^{e}} \left(\frac{\partial (\mathbf{L}_{\mathrm{p}})_{f}^{e}}{\partial \lambda} \Big|_{\text{explicit}} + \frac{\partial (\mathbf{L}_{\mathrm{p}})_{f}^{e}}{\partial v_{h}^{g}} \frac{\partial v_{h}^{g}}{\partial \Xi_{m}^{n}} \frac{\partial \Xi_{m}^{n}}{\partial \lambda} \right), \tag{57}$$

which yields directly the expression

$$\frac{\partial \Xi^n_m}{\partial \lambda} = \left(\delta^m_c \delta^d_n - \frac{\partial \Xi^d_c}{\partial (\mathbf{L}_\mathrm{p})^e_f} \frac{\partial (\mathbf{L}_\mathrm{p})^e_f}{\partial v^g_h} \frac{\partial v^g_h}{\partial \Xi^n_m} \right)^{-1} \frac{\partial \Xi^d_c}{\partial (\mathbf{L}_\mathrm{p})^e_f} \frac{\partial (\mathbf{L}_\mathrm{p})^e_f}{\partial \lambda} \bigg|_{\text{explicit}}. \tag{58}$$

It is important to point out that the term 'explicit' refers to the derivative of those terms which explicitly appear in the quantity with respect to which the derivative is considered. Note that in Eq. (58) the inverse of a fourth order tensor is to be performed.

In the following, we attend to the determination of the different terms involved in (58). Altogether we need to determine the following expressions: $\partial \mathbf{L}_\mathrm{p}/\partial\lambda|_{\text{explicit}}, \partial \boldsymbol{\Xi}/\partial \mathbf{L}_\mathrm{p}, (\partial \mathbf{L}_\mathrm{p}/\partial \boldsymbol{v})(\partial \boldsymbol{v}/\partial \boldsymbol{\Xi})$. For the sake of clarity this is done in the following sections.

3.1.1. The term $\partial \mathbf{L}_\mathrm{p}/\partial\lambda|_{\text{explicit}}$

The explicit derivative follows immediately from (36)

$$\frac{\partial (\mathbf{L}_\mathrm{p})^e_f}{\partial \lambda}\bigg|_{\text{explicit}} = \sqrt{\frac{2}{3}} \frac{\sigma^0_{11}}{2\sqrt{\chi}} \frac{\partial \chi}{\partial (\operatorname{dev} \boldsymbol{\Xi})^b_a} \frac{\partial (\operatorname{dev} \boldsymbol{\Xi})^b_a}{\partial \Xi^f_e} = v^e_f. \tag{59}$$

3.1.2. The term $\partial \boldsymbol{\Xi}/\partial \mathbf{L}_\mathrm{p}$

The derivative $\partial \boldsymbol{\Xi}/\partial \mathbf{L}_\mathrm{p}$ is derived using the chain rule by observing that $\boldsymbol{\Xi}$ depend on $\mathbf{L}_\mathrm{p}$ through its dependency on $\mathbf{F}^{-1}_\mathrm{p}$. One has first

$$\frac{\partial \Xi^j_i}{\partial (\mathbf{L}_\mathrm{p})^k_l} = \frac{\partial \Xi^j_i}{\partial (\mathbf{F}^{-1}_\mathrm{p})^r_s} \frac{\partial (\mathbf{F}^{-1}_\mathrm{p})^r_s}{\partial (\mathbf{L}_\mathrm{p})^k_l}. \tag{60}$$

Each term in this equation is considered individually and will be discussed in the following paragraphs.

3.1.2.1. The term $\partial \boldsymbol{\Xi}/\partial \mathbf{F}^{-1}_\mathbf{p}$.

$\boldsymbol{\Xi}$ depends on $\mathbf{F}^{-1}_\mathrm{p}$ via its dependency on $\mathbf{C}^{-1}_\mathrm{p}$ and ${}_m\overline{\mathbf{M}}_\mathrm{e}$. From Eq. (15), we conclude

$$\begin{aligned}
\frac{\partial \Xi^j_i}{\partial (\mathbf{F}^{-1}_\mathrm{p})^r_s} = 2\rho_0 \Bigg\{ \sum_{m=1}^{3} \Bigg[& \frac{\partial^2 \psi}{\partial J_m \partial (\mathbf{F}^{-1}_\mathrm{p})^r_s} (\mathbf{C}\mathbf{C}^{-1}_\mathrm{p})^a_i ({}_m\overline{\mathbf{M}}_\mathrm{e})^j_a + \frac{\partial \psi}{\partial J_m} \left(\frac{\partial (\mathbf{C}\mathbf{C}^{-1}_\mathrm{p})^a_i}{\partial (\mathbf{F}^{-1}_\mathrm{p})^s_r} ({}_m\overline{\mathbf{M}}_\mathrm{e})^j_a + (\mathbf{C}\mathbf{C}^{-1}_\mathrm{p})^a_i \frac{\partial ({}_m\overline{\mathbf{M}}_\mathrm{e})^j_a}{\partial (\mathbf{F}^{-1}_\mathrm{p})^s_r} \right) \\
& + \frac{\partial \psi}{\partial J_{m+3}} \left(\frac{\partial (\mathbf{C}\mathbf{C}^{-1}_\mathrm{p})^a_i}{\partial (\mathbf{F}^{-1}_\mathrm{p})^s_r} ({}_m\overline{\mathbf{M}}_\mathrm{e})^b_a (\mathbf{C}\mathbf{C}^{-1}_\mathrm{p})^j_b + (\mathbf{C}\mathbf{C}^{-1}_\mathrm{p})^a_i ({}_m\overline{\mathbf{M}}_\mathrm{e})^b_a \frac{\partial (\mathbf{C}\mathbf{C}^{-1}_\mathrm{p})^j_b}{\partial (\mathbf{F}^{-1}_\mathrm{p})^s_r} + (\mathbf{C}\mathbf{C}^{-1}_\mathrm{p})^a_i \frac{\partial ({}_m\overline{\mathbf{M}}_\mathrm{e})^b_a}{\partial (\mathbf{F}^{-1}_\mathrm{p})^s_r} (\mathbf{C}\mathbf{C}^{-1}_\mathrm{p})^j_b \right. \\
& \left. + (\mathbf{C}\mathbf{C}^{-1}_\mathrm{p})^a_i (\mathbf{C}\mathbf{C}^{-1}_\mathrm{p})^b_a \frac{\partial ({}_m\overline{\mathbf{M}}_\mathrm{e})^j_b}{\partial (\mathbf{F}^{-1}_\mathrm{p})^s_r} + \frac{\partial (\mathbf{C}\mathbf{C}^{-1}_\mathrm{p})^a_i}{\partial (\mathbf{F}^{-1}_\mathrm{p})^s_r} (\mathbf{C}\mathbf{C}^{-1}_\mathrm{p})^b_a ({}_m\overline{\mathbf{M}}_\mathrm{e})^j_b + (\mathbf{C}\mathbf{C}^{-1}_\mathrm{p})^a_i \frac{\partial (\mathbf{C}\mathbf{C}^{-1}_\mathrm{p})^b_a}{\partial (\mathbf{F}^{-1}_\mathrm{p})^s_r} ({}_m\overline{\mathbf{M}}_\mathrm{e})^j_b \right) \Bigg] \Bigg\}.
\end{aligned} \tag{61}$$

The derivatives $\partial\psi/\partial J_m$ can be easily provided. Eq. (13) yields

$$\rho_0 \frac{\partial \psi_\mathrm{e}}{\partial J_1} = \alpha_1 + \alpha_4 J_1 + \alpha_7 J_2 + \alpha_8 J_3, \tag{62}$$

$$\rho_0 \frac{\partial \psi_\mathrm{e}}{\partial J_2} = \alpha_2 + \alpha_5 J_2 + \alpha_7 J_1 + \alpha_9 J_3, \tag{63}$$

$$\rho_0 \frac{\partial \psi_\mathrm{e}}{\partial J_3} = \alpha_3 + \alpha_6 J_3 + \alpha_8 J_1 + \alpha_9 J_2, \tag{64}$$

$$\rho_0 \frac{\partial \psi_\mathrm{e}}{\partial J_4} = \alpha_{10}, \tag{65}$$

$$\rho_0 \frac{\partial \psi_\mathrm{e}}{\partial J_5} = \alpha_{11}, \tag{66}$$

$$\rho_0 \frac{\partial \psi_\mathrm{e}}{\partial J_6} = \alpha_{12}. \tag{67}$$

The same is true for the second derivative of the above expressions with respect to $\mathbf{F}_{\mathrm{p}}^{-1}$:

$$\frac{\partial^2\psi}{\partial(J_m)\partial(\mathbf{F}_{\mathrm{p}}^{-1})_s^r} = \left\{ \begin{array}{l} \alpha_4 \frac{\partial J_1}{\partial(\mathbf{F}_{\mathrm{p}}^{-1})_s^r} + \alpha_7 \frac{\partial J_2}{\partial(\mathbf{F}_{\mathrm{p}}^{-1})_s^r} + \alpha_8 \frac{\partial J_3}{\partial(\mathbf{F}_{\mathrm{p}}^{-1})_s^r}, \\ \alpha_5 \frac{\partial J_2}{\partial(\mathbf{F}_{\mathrm{p}}^{-1})_s^r} + \alpha_7 \frac{\partial J_1}{\partial(\mathbf{F}_{\mathrm{p}}^{-1})_s^r} + \alpha_9 \frac{\partial J_3}{\partial(\mathbf{F}_{\mathrm{p}}^{-1})_s^r}, \\ \alpha_6 \frac{\partial J_3}{\partial(\mathbf{F}_{\mathrm{p}}^{-1})_s^r} + \alpha_8 \frac{\partial J_1}{\partial(\mathbf{F}_{\mathrm{p}}^{-1})_s^r} + \alpha_9 \frac{\partial J_2}{\partial(\mathbf{F}_{\mathrm{p}}^{-1})_s^r}. \end{array} \right\},$$

where we have, using (14),

$$\frac{\partial J_m}{\partial(\mathbf{F}_{\mathrm{p}}^{-1})_s^r} = ({}_m\mathbf{M}_{\mathrm{e}})^{ns}(\mathbf{C})_{ru}(\mathbf{F}_{\mathrm{p}}^{-1})_n^u + ({}_m\mathbf{M}_{\mathrm{e}})^{sn}(\mathbf{F}_{\mathrm{p}}^{-1})_n^t(\mathbf{C})_{tr}, \quad i = 1,2,3. \tag{68}$$

Further we need the expression

$$\frac{\partial(\mathbf{C}\mathbf{C}_{\mathrm{p}}^{-1})_i^a}{\partial(\mathbf{F}_{\mathrm{p}}^{-1})_s^r} = (\mathbf{C})_{ir}(\mathbf{F}_{\mathrm{p}}^{-1})^{as} + (\mathbf{C})_{iu}(\mathbf{F}_{\mathrm{p}}^{-1})^{us}\delta_r^a, \tag{69}$$

and, finally, by taking into consideration the expression of the modified structural tensors (Eq. (16)), one has

$$\frac{\partial({}_m\overline{\mathbf{M}}_{\mathrm{e}})_a^b}{\partial(\mathbf{F}_{\mathrm{p}}^{-1})_s^r} = -(\mathbf{F}_{\mathrm{p}})_a^s({}_m\overline{\mathbf{M}}_{\mathrm{e}})_r^b + (\mathbf{F}_{\mathrm{p}}^{\mathrm{T}}{}_m\mathbf{M}_{\mathrm{e}})_a^s\delta_r^b. \tag{70}$$

This completes the determination of $\partial\boldsymbol{\Xi}/\partial\mathbf{F}_{\mathrm{p}}^{-1}$.

3.1.2.2. The term $\partial\mathbf{F}_{\mathrm{p}}^{-1}/\partial\mathbf{L}_{\mathrm{p}}$. The second derivative on the right hand side of (60) is established using (48). One has

$$\frac{\partial(\mathbf{F}_{\mathrm{p}}^{-1})_s^r}{\partial(\mathbf{L}_{\mathrm{p}})_l^k} = \frac{\partial(\mathbf{F}_{\mathrm{p}}^{-1})_s^r}{\partial[\exp(-\Delta T\mathbf{L}_{\mathrm{p}})]_f^e}\frac{\partial[\exp(-\Delta T\mathbf{L}_{\mathrm{p}})]_f^e}{\partial(-\Delta T\mathbf{L}_{\mathrm{p}})_h^g}\frac{\partial(-\Delta T\mathbf{L}_{\mathrm{p}})_h^g}{\partial(\mathbf{L}_{\mathrm{p}})_l^k}, \tag{71}$$

as well as

$$\frac{\partial(\mathbf{F}_{\mathrm{p}}^{-1})_s^r}{\partial[\exp(-\Delta T\mathbf{L}_{\mathrm{p}})]_f^e} = (\mathbf{F}_{\mathrm{p}}^{-1}|_n)_s^f\delta_e^r. \tag{72}$$

The second term on the right hand side of (71) is the tangent of the exponential map with respect to its argument resulting in a fourth order tensor. We consider an expression derived in [16] which is denoted by $\boldsymbol{\Upsilon}$. Altogether one has

$$\frac{\partial(\mathbf{F}_{\mathrm{p}}^{-1})_s^r}{\partial(\mathbf{L}_{\mathrm{p}})_l^k} = -\Delta T\Upsilon^r{}_{fk}{}^l(\mathbf{F}_{\mathrm{p}}^{-1}|_n)_s^f, \tag{73}$$

which completes, together with the results of the last section, the determination of $\partial\boldsymbol{\Xi}/\partial\mathbf{L}_{\mathrm{p}}$.

3.1.3. The term $(\partial\mathbf{L}_{\mathrm{p}}/\partial\boldsymbol{v})(\partial\boldsymbol{v}/\partial\boldsymbol{\Xi})$

In Eq. (58), we still need an expression for $(\partial\mathbf{L}_{\mathrm{p}}/\partial\boldsymbol{v})(\partial\boldsymbol{v}/\partial\boldsymbol{\Xi})$. First, we consider the derivative of $\mathbf{L}_{\mathrm{p}}$ with respect to $\boldsymbol{v}$. Using Eq. (36) one has

$$\frac{\partial(\mathbf{L}_{\mathrm{p}})_f^e}{\partial v_h^g} = \lambda. \tag{74}$$

By the very definition of $\boldsymbol{v}$, also Eq. (36), the following relations hold

$$\frac{\partial v_h^g}{\partial\Xi_m^n} = \sqrt{\frac{2}{3}}\frac{\sigma_{11}^0}{2\sqrt{\chi}}\left[\frac{\partial^2\chi}{\partial(\mathrm{dev}\,\boldsymbol{\Xi})_a^b\partial(\mathrm{dev}\,\boldsymbol{\Xi})_k^l}\frac{\partial(\mathrm{dev}\,\boldsymbol{\Xi})_a^b}{\partial\Xi_g^h} - \frac{1}{2\sqrt{\chi}}\frac{\partial\chi}{\partial(\mathrm{dev}\,\boldsymbol{\Xi})_a^b}\frac{\partial\chi}{\partial(\mathrm{dev}\,\boldsymbol{\Xi})_k^l}\frac{\partial(\mathrm{dev}\,\boldsymbol{\Xi})_a^b}{\partial\Xi_g^h}\right]\frac{\partial(\mathrm{dev}\,\boldsymbol{\Xi})_k^l}{\partial\Xi_m^n}. \tag{75}$$

While $\partial\chi/\partial \mathrm{dev}\,\boldsymbol{\Xi}$ is defined in Eq. (38), the second derivative is given as

$$\frac{\partial^2\chi}{\partial(\mathrm{dev}\,\boldsymbol{\Xi})^b_a\partial(\mathrm{dev}\,\boldsymbol{\Xi})^l_k} = \sum_{i=1}^{3}\left\{2\beta_i\left({}_i\mathbf{M}_y\right)^a_b\left({}_i\mathbf{M}_y\right)^k_l + \beta_{(i+6)}\left[\delta^k_b({}_i\mathbf{M}_y)^a_l + ({}_i\mathbf{M}_y)^k_b\delta^a_l\right] + \sum_{j=1}^{3}\left[\beta_{(i+j+1)}\left[({}_i\mathbf{M}_y)^k_l({}_j\mathbf{M}_y)^a_b + ({}_j\mathbf{M}_y)^k_l({}_i\mathbf{M}_y)^a_b\right]\right]\right\}, \tag{76}$$

where the condition $i \neq j$ has to be fulfilled. Finally, we have

$$\frac{\partial(\mathrm{dev}\,\boldsymbol{\Xi})^b_a}{\partial\Xi^f_e} = \delta^e_a\delta^b_f - \frac{1}{3}\delta^e_f\delta^b_a. \tag{77}$$

By now, all necessary ingredients to calculate $\partial\boldsymbol{\Xi}/\partial\lambda$ in Eq. (53) have been provided.

The previous sections give a clear picture of how much the local iteration in this general anisotropic setting differs from that of an isotropic one. In isotropic cases, local iterations, if any, are reduced to solving simple scalar equations.

3.2. The algorithmic tangent operator

In this section, the procedure for the computation of the algorithmic tangent operator is developed based on the systematic linearisation of the second Piola–Kirchhoff tensor $\mathbf{S}$ with respect to the right Cauchy–Green deformation tensor. The tensor $\mathbf{S}$ can be written as

$$\mathbf{S} = \mathbf{C}^{-1}\boldsymbol{\Xi}. \tag{78}$$

Accordingly, its linearisation takes the following form

$$\frac{\partial\mathbf{S}}{\partial\mathbf{C}} = \frac{\partial\mathbf{C}^{-1}}{\partial\mathbf{C}}\boldsymbol{\Xi} + \mathbf{C}^{-1}\frac{\partial\boldsymbol{\Xi}}{\partial\mathbf{C}}. \tag{79}$$

The first term on the right hand side is readily provided

$$\frac{\partial(\mathbf{C}^{-1})^{al}}{\partial(\mathbf{C})_{ij}}(\boldsymbol{\Xi})^b_l = -(\mathbf{C}^{-1})^{ai}(\mathbf{C}^{-1})^{jl}(\boldsymbol{\Xi})_l{}^b = -(\mathbf{C}^{-1})^{ai}(\mathbf{S})^{jb}. \tag{80}$$

The computation of the term $\partial\boldsymbol{\Xi}/\partial\mathbf{C}$ is based on the same ideas tested in the local iteration. One splits the derivative into explicit terms and implicit ones. The correct identification of the implicit dependencies is at the heart of the whole procedure. According to this, we may elaborate

$$\frac{\partial\Xi^b_a}{\partial(\mathbf{C})_{kl}} = \frac{\partial\Xi^b_a}{\partial(\mathbf{L}_\mathrm{p})^g_h}\frac{\partial(\mathbf{L}_\mathrm{p})^g_h}{\partial(\mathbf{C})_{kl}} + \left.\frac{\partial\Xi^b_a}{\partial(\mathbf{C})_{kl}}\right|_{\mathrm{explicit}}. \tag{81}$$

Herein, the term $\partial\boldsymbol{\Xi}/\partial\mathbf{L}_\mathrm{p}$ is identical to the term considered in Eq. (60) and evaluated in some sections of Section 3.1. The expression established in the last local iteration is the one which is to be used in the evaluation of (81). For clarity, further terms involved in (81) are evaluated in the following sections.

3.2.1. Evaluation of $\partial\boldsymbol{\Xi}/\partial\mathbf{C}|_{\mathrm{explicit}}$

We start with Eq. (15) which provides

$$\left.\frac{\partial\Xi^j_i}{\partial(\mathbf{C})_{kl}}\right|_{\mathrm{explicit}} = 2\rho_0\left\{\sum_{m=1}^{3}\left[\frac{\partial^2\psi}{\partial J_m\partial(\mathbf{C})_{kl}}(\mathbf{C}\mathbf{C}_\mathrm{p}^{-1})^a_i({}_m\overline{\mathbf{M}}_\mathrm{e})^j_a + \frac{\partial\psi}{\partial J_m}\frac{\partial(\mathbf{C}\mathbf{C}_\mathrm{p}^{-1})^a_i}{\partial(\mathbf{C})_{kl}}({}_m\overline{\mathbf{M}}_\mathrm{e})^j_a + \frac{\partial\psi}{\partial J_{(m+3)}}\left[\frac{\partial(\mathbf{C}\mathbf{C}_\mathrm{p}^{-1})^a_i}{\partial(\mathbf{C})_{kl}}({}_m\overline{\mathbf{M}}_\mathrm{e})^b_a(\mathbf{C}\mathbf{C}_\mathrm{p}^{-1})^j_b + (\mathbf{C}\mathbf{C}_\mathrm{p}^{-1})^a_i({}_m\overline{\mathbf{M}}_\mathrm{e})^b_a\frac{\partial(\mathbf{C}\mathbf{C}_\mathrm{p}^{-1})^j_b}{\partial(\mathbf{C})_{kl}} + \frac{\partial(\mathbf{C}\mathbf{C}_\mathrm{p}^{-1})^a_i}{\partial(\mathbf{C})_{kl}}(\mathbf{C}\mathbf{C}_\mathrm{p}^{-1})^b_a({}_m\overline{\mathbf{M}}_\mathrm{e})^j_b + (\mathbf{C}\mathbf{C}_\mathrm{p}^{-1})^a_i\frac{\partial(\mathbf{C}\mathbf{C}_\mathrm{p}^{-1})^b_a}{\partial(\mathbf{C})_{kl}}({}_m\overline{\mathbf{M}}_\mathrm{e})^j_b\right]\right]\right\}. \tag{82}$$

Using (62)–(67) the following derivatives can be established

$$\frac{\partial^2\psi}{\partial(J_i)\partial(\mathbf{C})_{kl}} = \begin{cases} \alpha_4 \frac{\partial J_1}{\partial(\mathbf{C})_{kl}} + \alpha_7 \frac{\partial J_2}{\partial(\mathbf{C})_{kl}} + \alpha_8 \frac{\partial J_3}{\partial(\mathbf{C})_{kl}}, \\ \alpha_5 \frac{\partial J_2}{\partial(\mathbf{C})_{kl}} + \alpha_7 \frac{\partial J_1}{\partial(\mathbf{C})_{kl}} + \alpha_9 \frac{\partial J_3}{\partial(\mathbf{C})_{kl}}, \\ \alpha_6 \frac{\partial J_3}{\partial(\mathbf{C})_{kl}} + \alpha_8 \frac{\partial J_1}{\partial(\mathbf{C})_{kl}} + \alpha_9 \frac{\partial J_2}{\partial(\mathbf{C})_{kl}}, \end{cases} \tag{83}$$

where we have

$$\frac{\partial J_i}{\partial(\mathbf{C})_{kl}} = ({}_i\mathbf{M}_{\mathrm{e}})^m_n (\mathbf{F}_{\mathrm{p}}^{-1})^k_m (\mathbf{F}_{\mathrm{p}}^{-1})^{ln}, \quad i = 1,2,3. \tag{84}$$

The last term to be defined in Eq. (82) is

$$\frac{\partial(\mathbf{C}\mathbf{C}_{\mathrm{p}}^{-1})^j_i}{\partial(\mathbf{C})_{kl}} = \delta^k_i (\mathbf{F}_{\mathrm{p}}^{-1})^l_b (\mathbf{F}_{\mathrm{p}}^{-1})^{jb}, \tag{85}$$

which completes the evaluation of $\partial\boldsymbol{\Xi}/\partial\mathbf{C}|_{\mathrm{explicit}}$.

3.2.2. Evaluation of $\partial\mathbf{L}_{\mathrm{p}}/\partial\mathbf{C}$

To evaluate Eq. (81) we still need the derivative of $\mathbf{L}_{\mathrm{p}}$ with respect to $\mathbf{C}$. The approach is based on obtaining an explicit expression for $\partial\boldsymbol{v}/\partial\mathbf{C}$ with the help of which the derivative $\partial\mathbf{L}_{\mathbf{p}}/\partial\mathbf{C}$ can be established. First, Eq. (36) results in

$$\frac{\partial(\mathbf{L}_{\mathrm{p}})^i_j}{\partial(\mathbf{C})_{rs}} = \left.\frac{\partial(\mathbf{L}_{\mathrm{p}})^i_j}{\partial\lambda}\right|_{\mathrm{explicit}} \frac{\partial\lambda}{\partial(\mathbf{C})_{rs}} + \left.\frac{\partial(\mathbf{L}_{\mathrm{p}})^i_j}{\partial v^a_b}\right|_{\mathrm{explicit}} \frac{\partial v^a_b}{\partial(\mathbf{C})_{rs}}, \tag{86}$$

$$\frac{\partial v^a_b}{\partial(\mathbf{C})_{rs}} = \frac{\partial v^a_b}{\partial\Xi^d_c}\left[\left.\frac{\partial\Xi^d_c}{\partial(\mathbf{C})_{rs}}\right|_{\mathrm{explicit}} + \frac{\partial\Xi^d_c}{\partial(\mathbf{L}_{\mathrm{p}})^e_f}\frac{\partial(\mathbf{L}_{\mathrm{p}})^e_f}{\partial(\mathbf{C})_{rs}}\right]. \tag{87}$$

Inserting (86) into (87) yields

$$\frac{\partial v^a_b}{\partial(\mathbf{C})_{rs}} = \frac{\partial v^a_b}{\partial\Xi^d_c}\left[\left.\frac{\partial\Xi^d_c}{\partial(\mathbf{C})_{rs}}\right|_{\mathrm{explicit}} + \frac{\partial\Xi^d_c}{\partial(\mathbf{L}_{\mathrm{p}})^e_f}\left(\left.\frac{\partial(\mathbf{L}_{\mathrm{p}})^e_f}{\partial\lambda}\right|_{\mathrm{explicit}}\frac{\partial\lambda}{\partial(\mathbf{C})_{rs}} + \left.\frac{\partial(\mathbf{L}_{\mathrm{p}})^e_f}{\partial v^g_h}\right|_{\mathrm{explicit}}\frac{\partial v^g_h}{\partial(\mathbf{C})_{rs}}\right)\right]. \tag{88}$$

Note that we could not have solved for $\partial\mathbf{L}_{\mathrm{p}}/\partial\mathbf{C}$ should we have inserted (87) into (86), since $\partial\lambda/\partial\mathbf{C}$ itself is also a function of $\partial\mathbf{L}_{\mathrm{p}}/\partial\mathbf{C}$ as will be shown shortly. The following simple relations hold for the explicit derivatives:

$$\left.\frac{\partial(\mathbf{L}_{\mathrm{p}})^i_j}{\partial v^a_b}\right|_{\mathrm{explicit}} = \lambda\delta^i_a\delta^b_j, \quad \left.\frac{\partial(\mathbf{L}_{\mathrm{p}})^e_f}{\partial\lambda}\right|_{\mathrm{explicit}} = v^e_f. \tag{89}$$

What we still need is the derivative of the scalar λ with respect to $\mathbf{C}$. This is obtained by taking the derivative of the yield function, defined in Eq. (30), with respect to $\mathbf{C}$. One has first

$$\frac{\partial\phi}{\partial(\mathbf{C})_{rs}} = \frac{\partial\phi}{\partial\Xi^b_a}\frac{\partial\Xi^b_a}{\partial(\mathbf{L}_{\mathrm{p}})^c_d}\frac{\partial(\mathbf{L}_{\mathrm{p}})^c_d}{\partial v^e_f}\frac{\partial v^e_f}{\partial(\mathbf{C})_{rs}} + \left.\frac{\partial\phi}{\partial\Xi^b_a}\frac{\partial\Xi^b_a}{\partial(\mathbf{C})_{rs}}\right|_{\mathrm{explicit}} + \frac{\partial\phi}{\partial\lambda}\frac{\partial\lambda}{\partial(\mathbf{C})_{rs}} = (\mathbf{0})^{rs}, \tag{90}$$

which, together with (89), results in

$$\frac{\partial\lambda}{\partial(\mathbf{C})_{rs}} = \frac{1}{-\frac{\partial\phi}{\partial\lambda}}\left[\lambda\frac{\partial\phi}{\partial\Xi^b_a}\frac{\partial\Xi^b_a}{\partial(\mathbf{L}_{\mathrm{p}})^c_d}\frac{\partial v^c_d}{\partial(\mathbf{C})_{rs}} + \frac{\partial\phi}{\partial\Xi^b_a}\left.\frac{\partial\Xi^b_a}{\partial(\mathbf{C})_{rs}}\right|_{\mathrm{explicit}}\right]. \tag{91}$$

The derivatives $\partial\phi/\partial\lambda$ and $\partial\phi/\partial\boldsymbol{\Xi}$ have been considered in Section 3.1. Their values are available from the last local iteration step. Eq. (91) is now inserted into (88) and the resulting equation is solved for the term $\partial\boldsymbol{v}/\partial\mathbf{C}$:

$$\frac{\partial v_g^h}{\partial(\mathbf{C})_{rs}} = \left[\delta_g^a\delta_b^h - \frac{\partial v_b^a}{\partial \Xi_c^d}\frac{\partial \Xi_c^d}{\partial(\mathbf{L}_p)_f^e}\left(\frac{\lambda}{-\frac{\partial\phi}{\partial\lambda}}v_f^e\frac{\partial\phi}{\partial\Xi_u^v}\frac{\partial\Xi_u^v}{\partial(\mathbf{L}_p)_h^g} + \lambda\delta_g^e\delta_f^h\right)\right]^{-1}\left(\frac{\partial v_b^a}{\partial\Xi_c^d}\frac{\partial\Xi_c^d}{\partial(\mathbf{L}_p)_f^e}v_f^e\frac{1}{-\frac{\partial\phi}{\partial\lambda}}\frac{\partial\phi}{\partial\Xi_u^v} + \frac{\partial v_b^a}{\partial\Xi_u^v}\right)\frac{\partial\Xi_u^v}{\partial(\mathbf{C})_{rs}}\bigg|_{\text{explicit}}. \tag{92}$$

Note that all terms involved in this equation are either known or has been provided in the last step of the local iteration: the derivative $\partial\boldsymbol{v}/\partial\boldsymbol{\Xi}$ is established in (75), $\partial\boldsymbol{\Xi}/\partial\mathbf{L}_p$ is determined through (60), $\partial\phi/\partial\boldsymbol{\Xi}$ is readily available through (38), and $\partial\boldsymbol{\Xi}/\partial\mathbf{C}|_{\text{explicit}}$ is calculated in Section 3.2.1. Hence, $\partial\boldsymbol{v}/\partial\mathbf{C}$ can be evaluated. The evaluation necessitates the inversion of a fourth order tensor. With this result at hand we can solve Eq. (91). Having established the expressions for $\partial\boldsymbol{v}/\partial\mathbf{C}$ and $\partial\lambda/\partial\mathbf{C}$ we can evaluate Eq. (86) and finally, with that expression we can solve for Eq. (81), which results in the exact expression for the consistent elastoplastic tangent operator as formulated in (79).

Note that the tangent operator is non-symmetric in general. The loss of symmetry is not a direct consequence of the anisotropy itself but a consequence of the fact that the multiplicative structure of the theory that results directly from the multiplicative decomposition of the deformation gradient, together with the developed integration scheme.

4. Numerical examples

The integration algorithms presented so far have been implemented in a code for shell finite element computations. The shell theory and the finite element formulation have been presented in [14,16]. The shell formulation is based on a seven-parameter theory which includes transversal strains and thus enables the application of a complete three-dimensional constitutive law. The enhanced strain concept is applied to avoid locking phenomena.

The level of complexity exhibited by the tangent operator restricts the time steps for which convergence is achieved in the case of complex deformations. In the examples to follow (two- and three-dimensional), some 500 time steps have been used to arrive at the final deformed configuration.

4.1. Uniaxial tensile test

Lademo et al. [7] performed experiments on aluminum alloy AA7108-T1 specimen, Fig. 1. The main idea was to investigate the influence of the main material directions on the material parameters. Several experiments are performed where the specimens directions are rotated for 0°, 35°, 45°, 55° and 90° relative to the extrusion direction. In order to compare the numerical and the experimental results, the model is computed for different position of the material axes (0°, 12°, 25°, 35°, 45°, 55°, 75° and 90°), see Fig. 2. The following material parameters for the numerical model are considered according to the ones identified in [7]

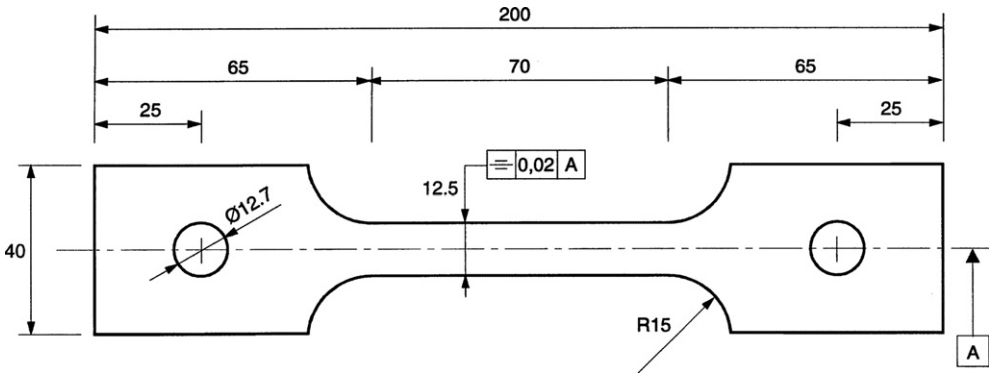

Fig. 1. Uniaxial tensile test: geometry of specimen used for experimental test, from [7].

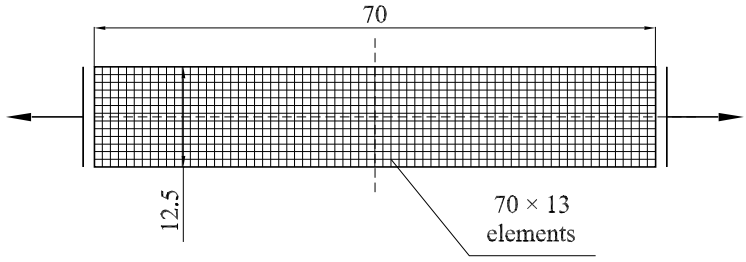

Fig. 2. Uniaxial tensile test: geometry of numerical model and material data.

$E_1 = 68135$ MPa, $E_2 = 69316$ MPa, $E_3 = 68135$ MPa,
$\nu_{12} = 0.32$, $\nu_{12} = 0.32$, $\nu_{12} = 0.32$,
$G_{12} = G_{13} = G_{23} = 25808.7$ MPa,
$\sigma_{11} = 295$ MPa, $\sigma_{22} = 263$ MPa, $\sigma_{33} = 215.8$ MPa,
$\sigma_{12} = 120.69$ MPa, $\sigma_{13} = 140.69$ MPa, $\sigma_{23} = 140.69$ MPa,
$H = 0$ MPa.

A comparison of the numerically and experimentally obtained curves, representing yield stresses in different directions, is presented in Fig. 3. As can be noticed, the results are in good agreement.

4.2. Isoerror maps

In order to get some insight into the accuracy of the numerical algorithm, isoerror maps are developed as described in [18]. Despite its lack of mathematical rigor, the procedure provides a quick numerical assessment of the accuracy of the integration algorithm.

Three points on the yield surface are selected which represent a wide range of possible states of stress. These points, labeled A, B and C, see Fig. 4, correspond to uniaxial, biaxial and pure shear stress states, respectively. In these cases, one element is loaded to the state A, B or C and than various combinations of strain increments $(\Delta\varepsilon_1, \Delta\varepsilon_2)$ are applied in a single step. Next, the 'exact' stresses are calculated for the same strain increment by subdividing the increments until further refinement produces negligible changes in the calculated stresses (in this case 1000 subincrements are made). Results are reported in terms of the relative root mean square of the error between 'exact' ($\mathbf{S}_*$) and computed solution ($\mathbf{S}$) according to the expression

$$\delta = \frac{\sqrt{[(\mathbf{S}-\mathbf{S}_*) : (\mathbf{S}-\mathbf{S}_*)]}}{\sqrt{(\mathbf{S}_* : \mathbf{S}_*)}} \times 100.$$

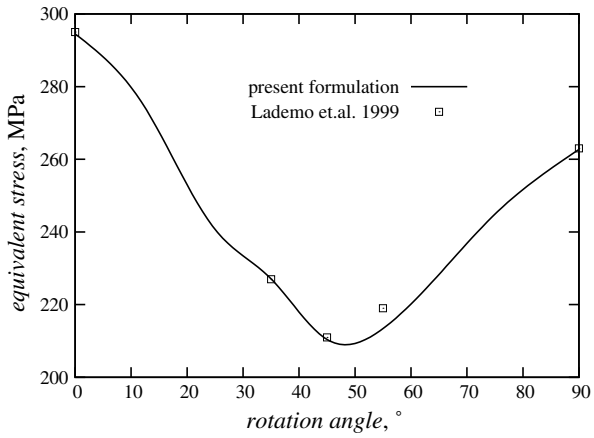

Fig. 3. Uniaxial tensile test: comparison of numerical and experimental results.

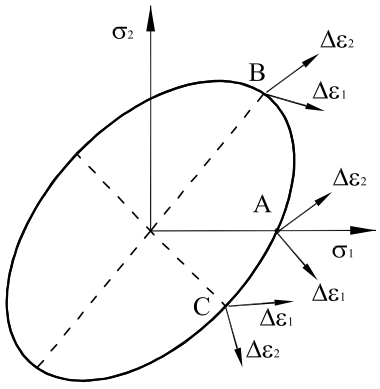

Fig. 4. Isoerror procedure: plane stress yield surface, from Simo and Taylor [18].

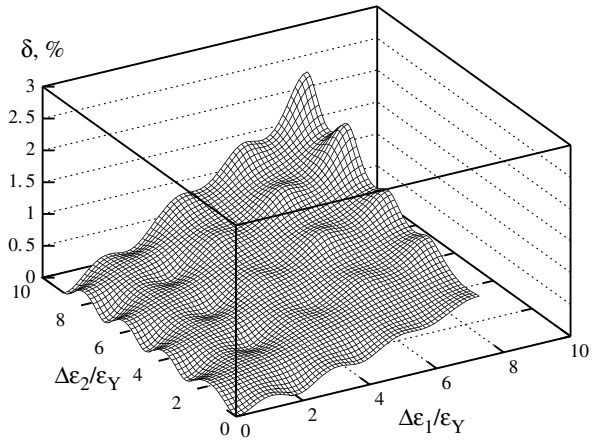

Fig. 5. Isoerror procedure: dependency of the numerical error on the strain increments in two directions for the load case A.

Computations are performed for an orthotropic material with the following parameters:

$$E_1 = 48042.7\ \text{MPa}, \quad E_2 = 41800\ \text{MPa}, \quad E_3 = 41800\ \text{MPa},$$
$$v_{12} = 0.2355, \quad v_{12} = 0.258, \quad v_{12} = 0.24,$$
$$G_{12} = 14214.0\ \text{MPa}, \quad G_{13} = 14804.0\ \text{MPa}, \quad G_{23} = 14804.0\ \text{MPa},$$
$$\sigma_{11} = 180\ \text{MPa}, \quad \sigma_{22} = 220\ \text{MPa}, \quad \sigma_{33} = 250\ \text{MPa},$$
$$\sigma_{12} = 187.02\ \text{MPa}, \quad \sigma_{13} = 127.02\ \text{MPa}, \quad \sigma_{23} = 127.02\ \text{MPa}.$$

Results are shown for different strain increment pairs. The strain increments are normalized with respect to the yield strain (ε_Y). Figs. 5–7 show the error of the numerical procedure for the three different load cases named A, B and C. As can be observed in all three cases the error is not larger than 3%. For example, in [8] largest error is up to 20%, in [1] it is between 1.4% and 3.5% or in [2] between 5% and 20%. However, it should be mentioned that while the first paper is isotropic in nature, the two others consider anisotropy within the small strain regime only.

4.3. Circular plate subjected to line load

The idea to this example is borrowed, though slightly modified, from Papadopoulos and Lu [11]. The formulation there is based on the additive decomposition of the logarithmic strain tensor. A circular plate of

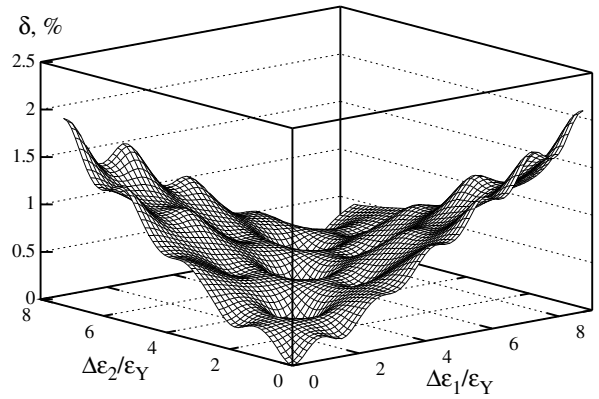

Fig. 6. Isoerror procedure: dependency of the numerical error on the strain increments in two directions for the load case B.

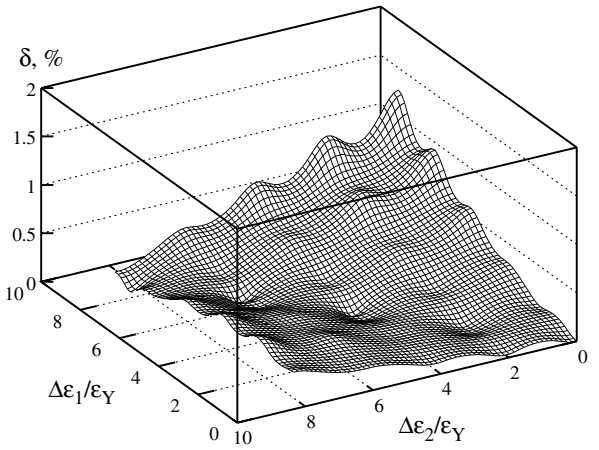

Fig. 7. Isoerror procedure: dependency of the numerical error on the strain increments in two directions for the load case C.

radius $R = 400$ mm and thickness $t = 10$ mm with a concentric hole of radius $R_i = 200$ mm is subjected to a line load of $q_z = 1000$ N/mm alongside the inner radius. Out of plane deformations are prevented so that only planar displacements and rotations can occur. Due to the geometrical and material symmetry one quarter of the plate is discretised with 10×10 elements. The material data and geometry of the plate are shown in Fig. 8.

Computations are performed for an elastically isotropic but plastically anisotropic material. The loading is presented in Fig. 6 but the computation itself is carried out until the maximum deformation, as shown in the figures, is reached.

Here three different sets of parameters are considered. This is determined by considering different ratios of the yield shear stress to the normal shear stress. In case A we have $\sigma^0_{12} = 0.5\sigma^0_{11}/\sqrt{3}$, in case B $\sigma^0_{12} = \sigma^0_{11}/\sqrt{3}$ (isotropic case) and in case C $\sigma^0_{12} = 2.0\sigma^0_{11}/\sqrt{3}$. The axes of anisotropy are defined to coincide with global axes 1 and 2. Fig. 9 shows deformed configurations for the three different case studies. As expected, in case A the plastic strains are concentrated in a direction at an angle of 45°, while in case C the concentration takes place in the direction of the material axes 1 and 2. In both anisotropic cases, the non-axiality between deformations and loading is clearly demonstrated.

4.4. Simply supported square plate

The elastoplastic deformation of a simply supported square plate is considered in the next example. The geometrical and material data is shown in Fig. 10, where the elastic response as well as the plastic one are

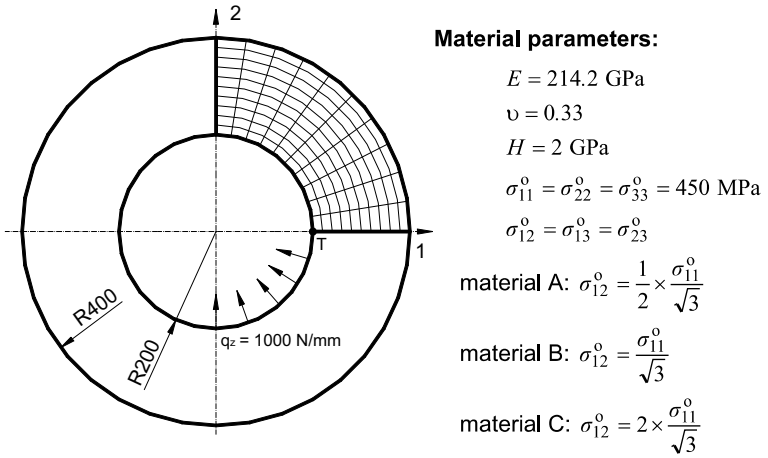

Fig. 8. Circular plate subjected to line load: geometrical and material parameters.

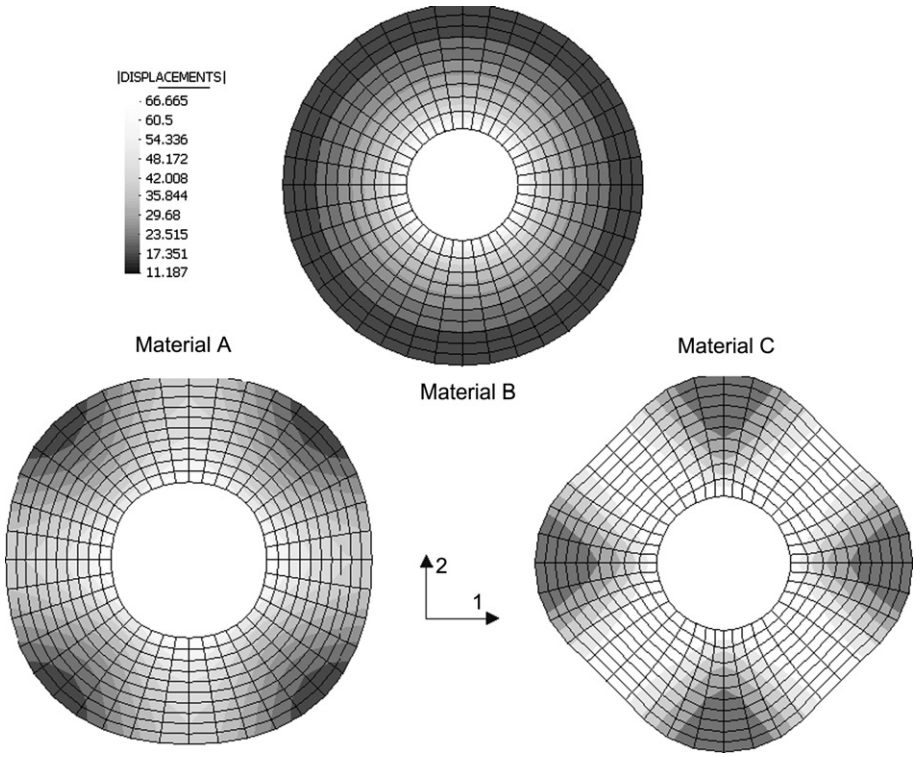

Fig. 9. Circular plate subjected to line load: deformed configuration.

assumed anisotropic. The privileged directions of both responses are assumed to coincide. The plate, subjected to a conservative constant transversal load, is supported at its boundaries in a way which does not allow for displacements in the out-of-plane direction to occur but allows for the boundary to undergo displacements in the plane itself. A finite element mesh of 35×35 is used to discretise the whole plate. The computation is carried out until the maximum deformations, as shown in the figures, are reached.

Figs. 11 and 12 show deformed configurations of the plate for different cases. In the cases under consideration, the privileged directions relative to the fixed co-ordinate system describe angles of 0°, 30°, 45°

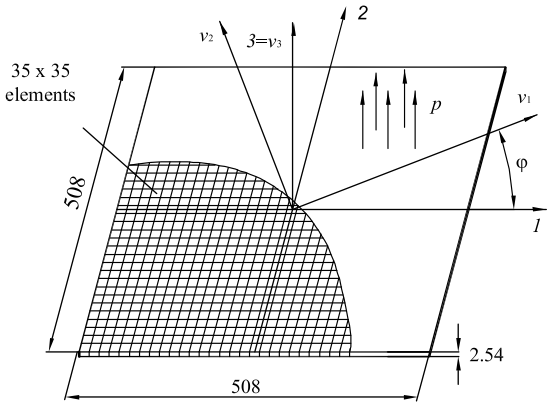

$E_1 = 210$ GPa, $E_2 = E_3 = 84$ GPa,
$\nu_{12} = 0.229$, $\nu_{13} = 0.243$, $\nu_{23} = 0.199$,
$G_{12} = G_{13} = 42$ G

and 60°. The isolines of the vertical displacement are plotted on these figures. A significant influence of the material privileged directions on the deformation process can be observed.

The load vs. vertical displacement curve plotted for the middle point is compared with the one obtained using the commercial finite element software package ABAQUS, Fig. 13. In ABAQUS, the used material model is based on the additive decomposition of the strain rate of the spatial logarithmic strain with the Green–Naghdi rate as the objective stress rate. Implemented are Hill's orthotropic yield criterion as well as an orthotropic elastic constitutive law. The formulation is restricted to small elastic strains. Two different directions of anisotropy are considered. As is clear from Fig. 13, the achieved results are compared with those from ABAQUS. Deviations become more pronounced at levels of larger deformations. However, we have to bear in mind that, while the theories are different we are still using same set of material parameters for either computation. As stated in the introduction, additive decompositions lack the rigour of the multiplicative decomposition and may produce physically questionable results as reported in [5]. However, the costs involved in computations based on the multiplicative decompositions are clearly much higher than those based on additive decompositions. This is expected since the mathematical structure of multiplicative anisotropy is by far much more complicated.

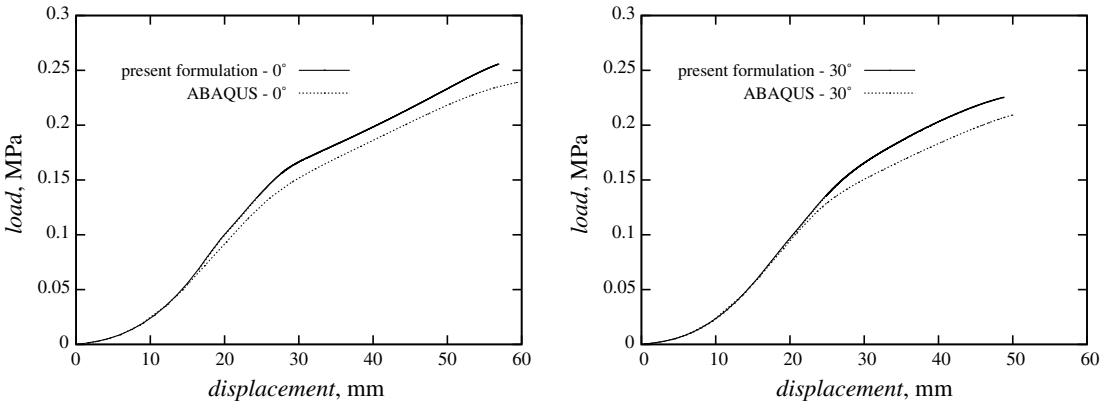

Fig. 13. Square plate: load vs. displacement curves at anisotropy angles $\varphi = 0°$ and 30° for two different formulations.

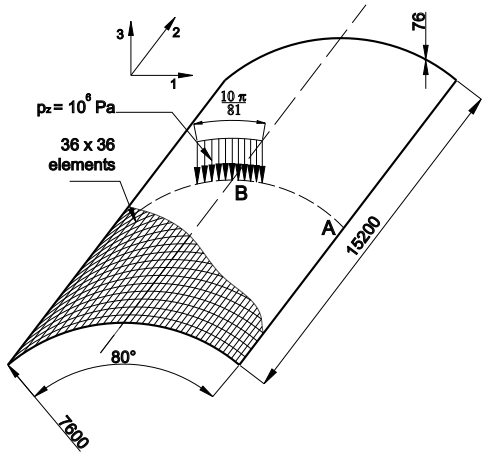

$E_1 = 48042.7$ MPa, $E_2 = 11800$ MPa, $E_3 = 11800$ MPa,
$\upsilon_{12} = 0.2355, \upsilon_{13} = 0.058, \upsilon_{23} = 0.34,$
$G_{12} = 4214$ MPa, $G_{13} = 4804$ MPa, $G_{23} = 4804$ MPa,
$\sigma^{o}_{11} = 220$ MPa, $\sigma^{o}_{22} = 220$ MPa, $\sigma^{o}_{33} = 220$ MPa

$$\sigma^{o}_{12} = \sigma^{o}_{13} = \sigma^{o}_{23} = \frac{1}{2} \times \frac{\sigma^{o}_{11}}{\sqrt{3}}$$

$H = 800$ MPa, $p_o = 10^3$ MPa

Fig. 14. Cylindrical roof: geometry and material data.

4.5. Cylindrical roof subjected to line load

As a third example, a cylindrical roof under line load is considered. The cylinder is supported by rigid diaphragms alongside the curved boundaries. The geometry and the material data are presented in Fig. 14. A finite element mesh of 36×36 elements has been employed. Here too elastic as well as plastic anisotropy are considered with the privileged directions of both responses assumed to coincide. We are taking local orientation of the axes in such a manner that for the computation defined by angle 0° privileged material directions coincide with circumferential, axial and radial direction of cylinder. In succeeding computations, the privileged directions are rotated for 30°, 45° and 60° with respect to the previously mentioned initial position. The influence of the material directions on the deformation responses is considered, and it is presented by load–displacement curves. Altogether 500 time steps has been calculated with 2–3 iterations in each time step.

Load factors (relative to the reference loading) vs. vertical displacements for two selected points A and B are plotted in Figs. 15 and 16. The deformed configurations of the cylindrical roof for the material axes of 0° and 45° are presented in Figs. 17 and 18. The isolines of the vertical displacement are plotted. As evident, a significant influence of the material directions on the elastoplastic deformation process is observed.

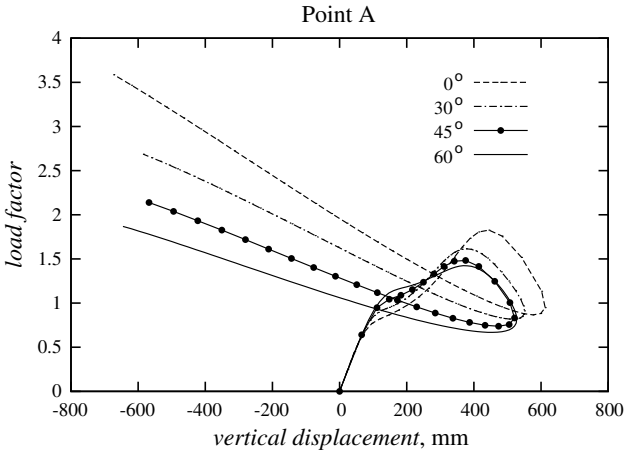

Fig. 15. Cylindrical roof: load vs. vertical displacement curves for point A.

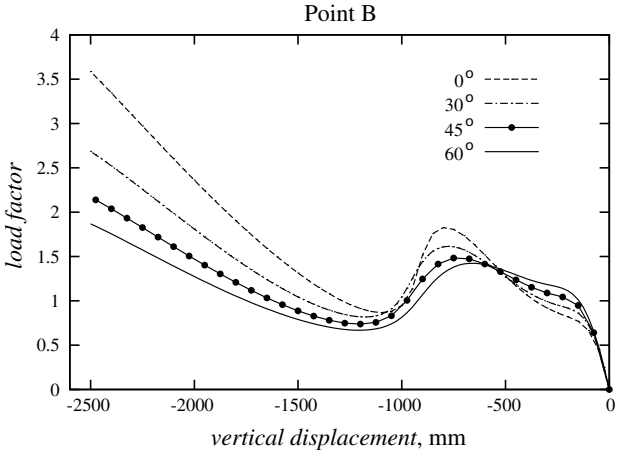

Fig. 16. Cylindrical roof: load vs. vertical displacement curves for point B.

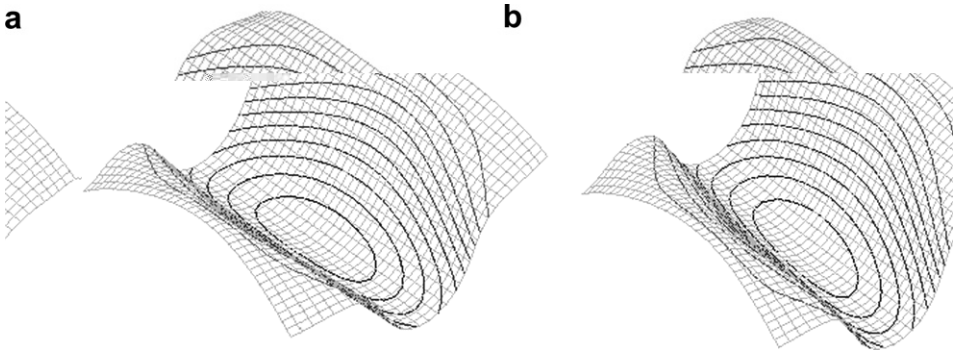

Fig. 17. Cylindrical roof: deformed configuration at 0° and 45° – isometric projection.

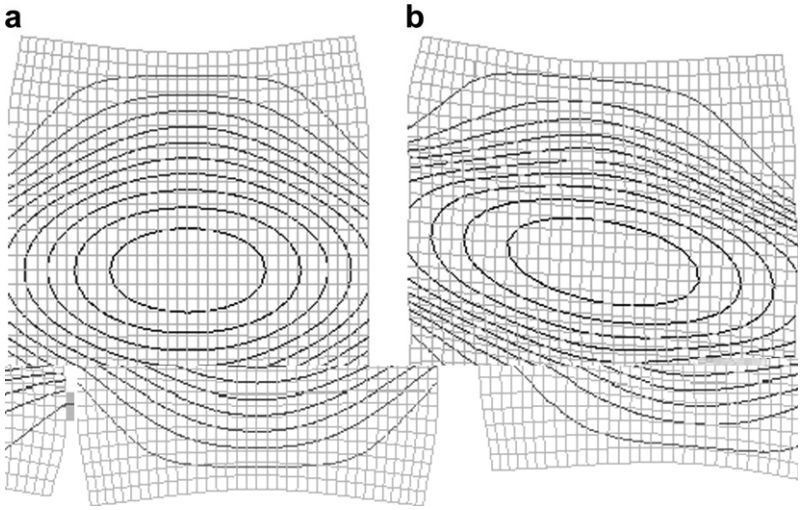

Fig. 18. Cylindrical roof: deformed configuration at 0° and 45° – plan projection.

5. Conclusion

A consistent large strain elastoplastic material model in the framework of multiplicative inelasticity was presented. The integration of the plastic rate was achieved by utilizing the exponential map which preserved the plastic incompressibility condition. To the first time, the consistent integration including the linearisation process for the anisotropic and multiplicative theoretical framework has been achieved. The details have been presented in full.

The numerical examples demonstrate a significant influence of anisotropy and the privileged directions on the deformation process. While the numerical algorithms have been, as demonstrated, successful, the numerical efforts are still considerable. The tangent operator renders non-symmetric and its computation asks for lengthy operations. This calls for the search for alternative integration schemes, which may at least preserve the symmetry of the tangent operator. Also the stability of the integration scheme with regard to the time step is an aspect which is worth an in-depth investigation.

On the theoretical side, the stored energy function is not invariant with respect to superimposed rotations on $\mathbf{F}_{\mathrm{p}}$. There are other rules and restrictions which could be imposed on such a function in order for it to exhibit such an invariance. The importance of the numerical implementation considered here is also reflected in the fact that the capabilities of such models can be tested and compared against each other. The implementation of alternative models is to be considered in future work.

References

[1] R.I. Borja, K.M. Sama, P.F. Sanz, Self-consistent Eulerian rate type elasto-plasticity models based upon the logarithmic stress rate, Computer Methods in Applied Mechanics and Engineering 192 (2003) 1227–1258.

[2] V. Cvitanić, F. Vlak, Z. Lozina, A finite element formulation based on non-associated plasticity for sheet metal forming, International Journal of Plasticity 24 (2008) 646–687.

[3] B. Eidel, F. Gruttmann, Elastoplastic orthotropy at finite strains: multiplicative formulation and numerical implementation, Computational Materials Science 28 (2003) 732–742.

[4] A.L. Eterovic, K.-J. Bathe, A hyperelastic-based large strain elasto-plastic constitutive formulation with combined isotropic-kinematic hardening using the logarithmic stress and strain measures, International Journal for Numerical Methods in Engineering 30 (1990) 1099–1114.

[5] M. Itskov, On the application of the additive decomposition of generalized strain measures in large strain plasticity, Mechanics Research Communications 31 (2004) 507–517.

[6] M. Itskov, N. Aksel, A constitutive model for orthotropic elasto-plasticity at large strains, Archive of Applied Mechanics (Ingenieur Archiv) 74 (2004) 75–91.

[7] O.G. Lademo, O.S. Hopperstadt, M. Langseth, An evaluation of yield criteria and flow rules for aluminium alloys, International Journal of Plasticity 15 (1999) 191–208.

[8] S.W. Lee, J.W. Yoon, D.Y. Yang, A stress integration algorithm for plane stress elastoplasticity and its applications to explicit finite element analysis of sheet metal forming processes, Computers and Structures 66 (1998) 301–311.

[9] J. Lemaitre, J.-L. Chaboche, Mechanics of Solid Materials, Cambridge University Press, London, 1990.

[10] A. Menzel, P. Steinmann, On the spatial formulation of anisotropic multiplicative elasto-plasticity, Computer Methods in Applied Mechanics and Engineering 192 (2003) 3431–3470.

[11] P. Papadopoulos, J. Lu, On the formulation and numerical solution of problems in anisotropic finite plasticity, Computer Methods in Applied Mechanics and Engineering 190 (2001) 4889–4910.

[12] C. Sansour, J. Bocko, On the numerical implications of multiplicative inelasticity with an anisotropic elastic constitutive law, International Journal for Numerical Methods in Engineering 58 (2003) 2131–2160.

[13] C. Sansour, I. Karšaj, J. Sorić, A formulation of anisotropic continuum elastoplasticity at finite strains. Part I: Modelling, International Journal of Plasticity 22 (2006) 2346–2365.

[14] C. Sansour, F.G. Kollmann, Large viscoplastic deformation of shells. Theory and finite element formulation, Computational Mechanics 21 (1998) 512–525.

[15] C. Sansour, F.G. Kollmann, Anisotropic formulations for finite strain viscoplasticity. Applications to shells, in: W.A. Wall, K.-U. Bletzinger, K. Schweizerhof (Eds.), Trends in Computational Structural Mechanics, CIMNE Barcelona, 2001, pp. 198–207.

[16] C. Sansour, W. Wagner, A model of finite strain viscoplasticity based on unified constitutive equations. Theoretical and computational considerations with applications to shells,Computer Methods in Applied Mechanics and Engineering 191 (2001) 423–450.

[17] J. Schroeder, F. Gruttmann, J. Löblein, A simple orthotropic finite elasto-plasticity model based on generalized stress–strain measures, Computational Mechanics 30 (2002) 38–64.

[18] J.C. Simo, R.L. Taylor, A return mapping algorithm for plane stress elastoplasticity, International Journal for Numerical Methods in Engineering 22 (1986) 649–670.

[19] G. Weber, L. Anand, Finite deformation constitutive equations and a time integration procedure for isotropic, hyperelastic–viscoplastic solids, Computer Methods in Applied Mechanics and Engineering 79 (1990) 173–202.